Effects of Surface Roughness and Surface Force on the Thin Film Elastohydrodynamic Lubrication of Circular Contacts

Li-Ming Chu[a], Jaw-Ren Lin[b], and Jiann-Lin Chen[a]

[a] Department of Mechanical and Automation Engineering, I-Shou University, Kaohsiung City 84001, Taiwan, R.O.C.

[b] Department of Mechanical Engineering, Taoyuan Innovation Institute of Technology, Jhongli City, Taoyuan County 320, Taiwan, R.O.C.

Reprint requests to L.-M. C.; Tel: 886-7-6577711ext3232, Fax: 886-7-6578853,
E-mail: hmchu@mail.isu.edu.tw

Z. Naturforsch. **67a,** 412 – 418 (2012) / DOI: 10.5560/ZNA.2012-0035
Received November 16, 2011 / revised February 6, 2012

The effects of surface roughness and surface force on thin film elastohydrodynamic lubrication (TFEHL) circular contact problems are analyzed and discussed under constant load condition. The multi-level multi-integration (MLMI) algorithm and the Gauss–Seidel iterative method are used to simultaneously solve the average Reynolds type equation, surface force equations, the load balance equation, the rheology equations, and the elastic deformation equation. The simulation results reveal that the difference between the TFEHL model and the traditional EHL model increase with decreasing film thickness. The effects of surface forces become significant as the film thickness becomes thinner. The surface forces have obvious effects in the Hertzian contact region. The oscillation phenomena in pressure and film thickness come mainly from the action of solvation forces.

Key words: Thin Film Elastohydrodynamic Lubrication (TFEHL); Roughness; Surface Force.

1. Introduction

Thin film lubrication (TFL) is indispensable as a basis of key technology in high technology devices and ultra-precision machines. Many experimental results [1, 2] show that the variations in the film thickness in the TFL regime are substantially different from those in the elastohydrodynamic lubrication (EHL) regime. The main contributions to these differences come from the effects of surface forces. In addition, the surface imposed during manufacturing is not perfectly smooth. The film may then be as thin as the asperities collide. In TFEHL problems, the film thickness is usually comparable to the height of the surface roughness. Therefore, it is important to estimate the pressure distribution and film thickness in the contact zone by taking into account the surface forces and surface roughness, for better understanding of TFEHL.

Nanotribological studies are necessary for the development of modern mechanical technology. The film thickness may be as small as several nanometers. Some interesting issues are raised after exploring the rheological properties of lubricants. The continuum hydrodynamic model remains valid down to 30 nm, and even down further to several nanometers, if a simple correction factor can be applied [3]. The attractive van der Waals force and oscillatory solvation forces begin to dominate at closer distances. In micro-EHL calculation, the composite topography as proposed by Brown and Scholz [4] is used to propose an exp-cos solvation force model [3] which is also applicable to the micro-EHL calculation by Jang and Tichy [5]. When the film thickness is very thin, the solvation force and the van der Waals force cannot be neglected. A new method for the EHL problem was proposed by Matsuoka and Kato [6]. By solving the transformed Ornstein–Zernike equation [7] for hard-spheres in a two-phase system with Perram's method [8], and by using the Derjaguin approximation, the solvation pressure is calculated. The effects of surface forces on the problems of a sphere pure squeeze on a plate have been discussed by Chu et al. [9].

In EHL contacts roughness and surface texture substantially affect the formation of a lubricating oil film between the contacting bodies. Therefore, the effects of surface roughness become important for thin film

lubrication as the standard derivation of the composite rough surfaces is comparable to the local film thickness. Two widely used tools are proposed for modelling the surface roughness: the stochastic analysis [10] and the deterministic analysis [11]. The deterministic model uses measured surface topography to calculate pressure distribution and film distribution. It takes time to trace all the asperities of the two lubricating surfaces to obtain the convergence of the solution. The statistic characteristics of a real rough surface can be mathematically approximated by a stochastic process with Gaussian height distribution. The Christensen's stochastic process theory [12] has been extended to EHL line contact and the effect of longitudinal roughness on the film thickness has been discussed [13]. The most commonly used approach is to solve the Reynolds equation with the assumption of smooth surfaces and use 'flow factors' to statistically compensate for the surface roughness. An average flow model [10] taking into account the asperity contact pressure calculated from the force compliance relationship derived by Greenwood and Tripp [14] has been used by several researchers [15, 16] to describe the effects of the surface roughness pattern, film factor, and operating conditions on the performance of EHL. The average flow model has the advantage of being easy to apply to distributed roughness problems. Several researchers [17, 18] have incorporated the effects of surface roughness into EHL analysis.

So far, the study on the effects of surface roughness and surface force on the TFEHL circular contact problems is not valid. The present analysis investigates the effects of surface roughness and surface force on the TFEHL circular contact problems numerically by solving seven equations simultaneously. The film thickness and pressure characteristics of the lubricant are discussed for various parameters.

2. Theoretical Analysis

2.1. Surface Forces Model

For interactions between solid surfaces in liquid, there are three important forces to be considered: van der Waals force, solvation force, and electrostatic double layer force. Electrostatic forces are related to the charging of a surface by the exchange of ions and are not considered. Surface forces act directly between the surfaces, but they are influenced by the pressure of the intervening liquid. The attractive van der Waals energy between two surfaces is decomposed in the form of a pressure distribution [19] as a function of local separation:

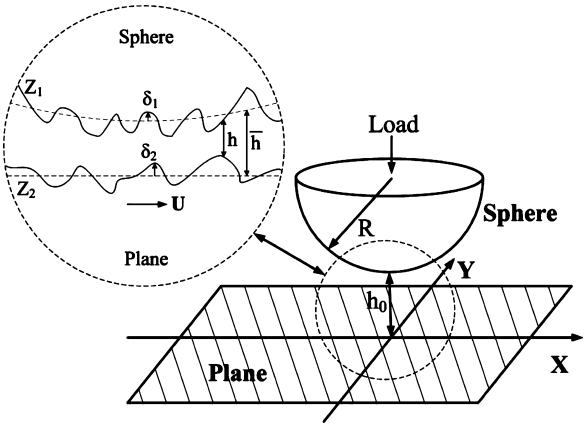

Fig. 1. Schematic of geometry of model problem.

$$p_{\mathrm{vdW}} \cong -\frac{10^{-19}}{6\pi h^3}\,. \tag{1}$$

The attractive force is treated as negative pressure.

The solvation force occurs whenever liquid molecules are introduced into a highly restricted gap and are forced to form a series of layers. According to molecular ordering in the gap, this force takes on an oscillatory and exponentially decaying function of separation. Following the exp-cos model for the solvation pressure on the analogy of characteristics of the solvation force referring to Chan and Horn's report [3], we can write

$$p_{\mathrm{solv}} = -C\exp\left(\frac{-h}{a}\right)\cos\left(\frac{2\pi h}{a}\right), \tag{2}$$

where p_{solv} is the solvation pressure, C is a constant, h is the surface separation, and a is the molecular diameter of the intervening liquid. Moreover, $a = 1.0$ nm and $C = 172$ MPa are used in the present analysis on the analogy of Chan and Horn [3] and Jang and Tichy [5]. The contact geometry of two balls can be reduced to the contact geometry of a ball and a flat surface as shown in Figure 1.

2.2. Average Type Reynolds Equations and Flow Factors

For the steady state, isothermal, EHL circular contact problems with effects of surface roughness taken

into account, the average type Reynolds equation [20] can be expressed in the following form:

$$\frac{\partial}{\partial x}\left(\frac{\rho h^3}{\eta}\phi_{xx}^p\frac{\partial p}{\partial x}\right)+\frac{\partial}{\partial y}\left(\frac{\rho h^3}{\eta}\phi_{yy}^p\frac{\partial p}{\partial y}\right) = 12\left[\bar{u}\frac{\partial \rho h}{\partial x}-u*\frac{\sigma}{2}\frac{\partial \rho \phi_{xx}^s}{\partial x}\right], \tag{3}$$

where

$$\bar{u}=\frac{u_2+u_1}{2}, \tag{4}$$

$$u^*=u_2-u_1. \tag{5}$$

The derived flow factors are

$$\phi_{xx}^p=1+3\left(\frac{\sigma}{h}\right)^2\left[1-\frac{3}{\gamma+1}\right], \tag{6}$$

$$\phi_{yy}^p=1+3\left(\frac{\sigma}{h}\right)^2\left[1-\frac{3\gamma}{\gamma+1}\right], \tag{7}$$

$$\phi_{xx}^s=-3\left(\frac{\sigma}{h}\right)\left[\left(\frac{\sigma_2}{\sigma}\right)^2\frac{1}{\gamma_2+1}-\left(\frac{\sigma_1}{\sigma}\right)^2\frac{1}{\gamma_1+1}\right], \tag{8}$$

with

$$\frac{1}{\gamma+1}=\left(\frac{\sigma_2}{\sigma}\right)^2\frac{1}{\gamma_2+1}+\left(\frac{\sigma_1}{\sigma}\right)^2\frac{1}{\gamma_1+1}, \tag{9}$$

$$\left(\frac{\sigma_2}{\sigma}\right)^2+\left(\frac{\sigma_1}{\sigma}\right)^2=1, \tag{10}$$

where σ is the standard deviation of composite roughness and γ the Peklenik parameter. Equation (3) can be expressed in the dimensionless form as

$$\frac{\partial}{\partial X}\left(\frac{\bar{\rho}H^3}{\bar{\eta}}\phi_{xx}^p\frac{\partial P}{\partial X}\right)+\frac{\partial}{\partial Y}\left(\frac{\bar{\rho}H^3}{\bar{\eta}}\phi_{yy}^p\frac{\partial P}{\partial Y}\right) = \lambda\left[\frac{\partial \bar{\rho}H}{\partial X}-\frac{u*\bar{\sigma}}{2\bar{u}}\frac{\partial \bar{\rho}\phi_{xx}^s}{\partial X}\right], \tag{11}$$

where

$$\lambda=\frac{12\eta_0\bar{u}R_x^2}{b^3p_h}. \tag{12}$$

The dimensionless parameters are represent to $X=x/b$, $Y=y/b$, $H=hR_x/b^2$, $P=p/p_h$, $\bar{\rho}=\rho/\rho_0$, $\bar{\eta}=\eta/\eta_0$, where $b=(3wR_x/2E')^{1/3}$ is the semiwidth of Hertzian contact, R_x the reduced radius of curvature in x-direction, η_0 the viscosity of the lubricant at ambient pressure, and ρ_0 the density of the lubricant at ambient pressure. $\bar{\eta}$ and $\bar{\rho}$ are dependent on the pressure. The boundary conditions for (11) are

$$P=0 \quad \text{at} \quad X=X_{\text{in}};\quad -1.8\le Y\le 1.8, \tag{13a}$$

$$P=0 \quad \text{at} \quad Y=\pm 1.8;\quad X_{\text{in}}\le X\le X_{end}=\varsigma(Y), \tag{13b}$$

$$P=\frac{\mathrm{d}P}{\mathrm{d}X}=0 \quad \text{at} \quad X=\varsigma(Y);\quad -1.8\le Y\le 1.8. \tag{13c}$$

2.3. Rheology Equation

The viscosity of the lubricant is assumed to be a function of pressure only. The relationship between viscosity and pressure used by Roelands et al. [21] can be expressed as

$$\bar{\eta}=\exp\{(9.67+\ln\eta_0)\cdot[-1+(1+5.1\times 10^{-9}p)^{z'}]\}, \tag{14}$$

where η_0 is the viscosity under ambient pressure and z' the pressure–viscosity index. According to Dowson and Higginson [22], the relationship between density and pressure is given as

$$\bar{\rho}=\frac{\rho}{\rho_0}=1+\frac{0.6\times 10^{-9}p}{1+1.7\times 10^{-9}p}. \tag{15}$$

2.4. Total Pressure

The hydrodynamic pressure p can be obtained by solving (3). The total pressure in this model is assumed to be the summation of the van der Waals, the solvation, and the hydrodynamic pressure:

$$p_{\text{total}}=p+p_{\text{solv}}+p_{\text{vdW}}. \tag{16}$$

The total pressure p_{total} in expression (16) is calculated simultaneously with the elasticity equations as in the conventional EHL theory. The pressure caused by surface forces as a function of film thickness is shown in Figure 2. Because of the interaction between the attraction pressure of the van der Waals force and the oscillating pressure of solvation, the surface pressure has the form of a sinusoidal function.

2.5. Film Equation

Using the parabolic approximation for the geometry, the lubricant film thickness in the dimensionless form

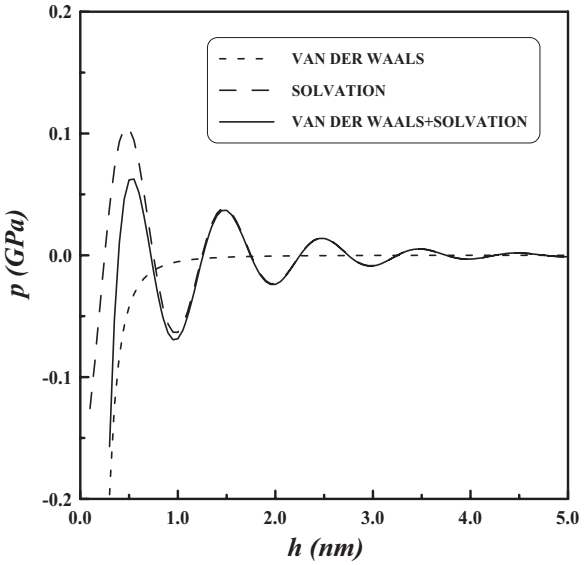

Fig. 2. Pressure due to surface forces as a function of film thickness.

can be written as

$$H(X,Y) = H_{00} + \frac{X^2+Y^2}{2} + \frac{2}{\pi^2}\int_{-\infty}^{\infty}\int_{-\infty}^{\infty}\frac{P_{\text{total}}(X',Y')\,\mathrm{d}X'\,\mathrm{d}Y'}{\left[(X-X')^2+(Y-Y')^2\right]^{1/2}}, \quad (17)$$

where H_{00} is a constant. Discretizing the elastic deformation integral, the film shape is given as

$$H_{i,j} = H_{00} + \frac{\left(X_{i,j}^2+Y_{i,j}^2\right)}{2} + \frac{2}{\pi^2}\sum_{k=1}^{n_x}\sum_{l=1}^{n_y}K_{ikjl}P_{\text{total}_{kl}}, \quad (18)$$

where the coefficients are determined analytically assuming a uniform pressure over the various rectangular areas in the contact area. The influence the coefficients K_{ikjl} is computed according to Lubrecht [23]. The assumption of roughness deformation is large for large wavelengths. The wavelength components deform almost completely by passing through the conjunction during the EHL process, while small wavelength components stay almost undeformed [24].

2.6. Force Balance Equation

The normal load on the ball is assumed to be constant, thus the constant H_{00} can be obtained from the dimensionless force balance equation:

$$\int_{-\infty}^{\infty}\int_{-\infty}^{\infty}P_{\text{total}}(X,Y)\,\mathrm{d}X\,\mathrm{d}Y = \frac{2\pi}{3}. \quad (19)$$

3. Results and Discussion

The material properties of lubricants and balls for the present analysis are listed in Table 1. The solutions of the film thickness and the pressure distributions of the isothermal EHL point-contact problems are obtained by solving the average Reynolds type equation, surface force equations, the load balance equation, the viscosity–pressure and density–pressure relations equations, and the elastic deformation equation simultaneously. The MLMI algorithm [25] and the Gauss–Seidel iterative method are used to solve the pressure and film thickness distributions of the TFEHL problem with effects of surface roughness and surface force. Most cases presented in this paper use a domain extending from $X_{\text{in}} = -4.0$ to $X_{\text{o}} = 1.4$ and $-1.8 \le Y \le 1.8$. The dimensionless outlet location $X_{\text{end}} = \varsigma(Y)$ is determined by the complementary theory of mathematical programming. A typical problem with $W = w/E'R_x^2 = 3.64133\times10^{-8}$, $U = \eta_0\bar{u}/E'R_x = 1.12244\times10^{-12}$, $G = 2416$, $\gamma_1 = \gamma_2 = \gamma = 0.1$, $\bar{\sigma} = \sigma R_x/b^2 = 0.020$, $\bar{\sigma}_1 = \bar{\sigma}_2 = 0.014$, and $S = -2.0$ is solved. A grid size of 33×97 grids in the half domain (symmetry *w.r.t.* X-axis) is used for evaluation of pressure and elastic deformation.

Figures 3a and 3b show the pressure and film thicknesses distributions including the van der Waals force and the solvation force in the case of $W = 3.64133\times10^{-8}$, $U = 1.12244\times10^{-12}$, $G = 2416$, $\gamma_1 = \gamma_2 = \gamma = 0.1$, $\bar{\sigma} = 0.020$, $\bar{\sigma}_1 = \bar{\sigma}_2 = 0.014$, and $S = -2.0$. It is interesting to find the pressure spike and the oscillatory phenomenon as shown in Figure 3a. The associated film shape is shown in Figure 3b. The pressure

Table 1. Computational data.

G (material parameter)	2416
Inlet viscosity of lubricant, Pa s	0.0411
Inlet density of lubricant, kg/m^3	846
Pressure–viscosity coefficient, 1/GPa	11.00
Pressure–viscosity index (Roelands)	0.3329
Equivalent radius, m	0.0005
Density of balls, kg/m^3	7850
Elastic modulus of balls, GPa	200
Poisson's ratio of balls	0.3

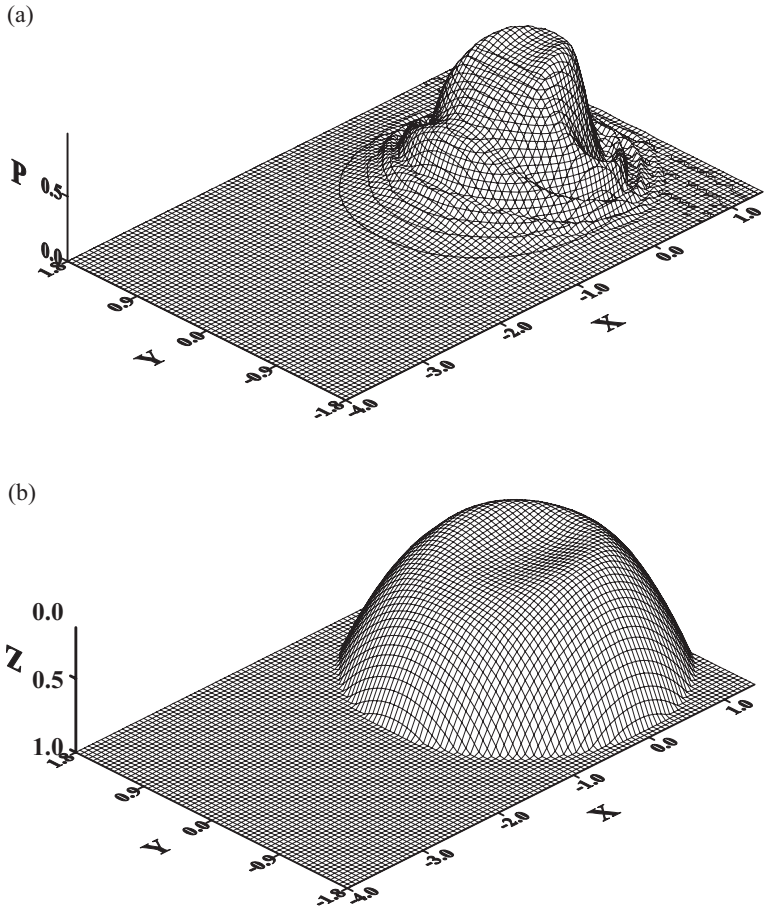

Fig. 3. 3D plot of pressure distribution (a) and film thickness (b).

spike and U-shaped region are the main characteristic of EHL.

Figures 4a and 4b show the pressure and film thickness distributions in x- and y-direction calculated by the surface forces model and the classical EHL model, respectively. It can be seen that the surface forces increase with decreasing film thickness. The surface forces have obvious effects in the Hertzian contact region. The solvation pressure oscillates as the film thickness varies, but the van der Waals pressure is almost zero. The hydrodynamic pressure is greater than the solvation pressure and the van der Waals pressure. Due to the oscillating nature of solvation pressure, the hydrodynamic pressure calculated from the TFEHL model is oscillating. The oscillation nature of solvation pressure causes film thickness oscillations. The hydrodynamic pressure calculated from the TFEHL model is slightly larger than the hydrodynamic pressure computed from the classical EHL model in the inlet and outlet regions. However, the hydrodynamic pressure calculated from the TFEHL model is smaller than the hydrodynamic pressure computed from the classical EHL model in the Hertzian contact region, except for a few central points. When the surface forces are added, the total pressure will relate differently to the classical EHL pressure. It is found that the difference is more apparent in the Hertzian contact region. The total pressure is also in the oscillating form in all regions. Particularly, the difference is the greatest when the thickness is the least. In addition, the differences in film thickness distribution between the traditional EHL model and the TFEHL model increase with decreasing film thickness. Due to the effect of surface forces, the film thickness is different as compared to the classical EHL film thickness. It is found that the deviation is more apparent in the Hertzian contact region. The de-

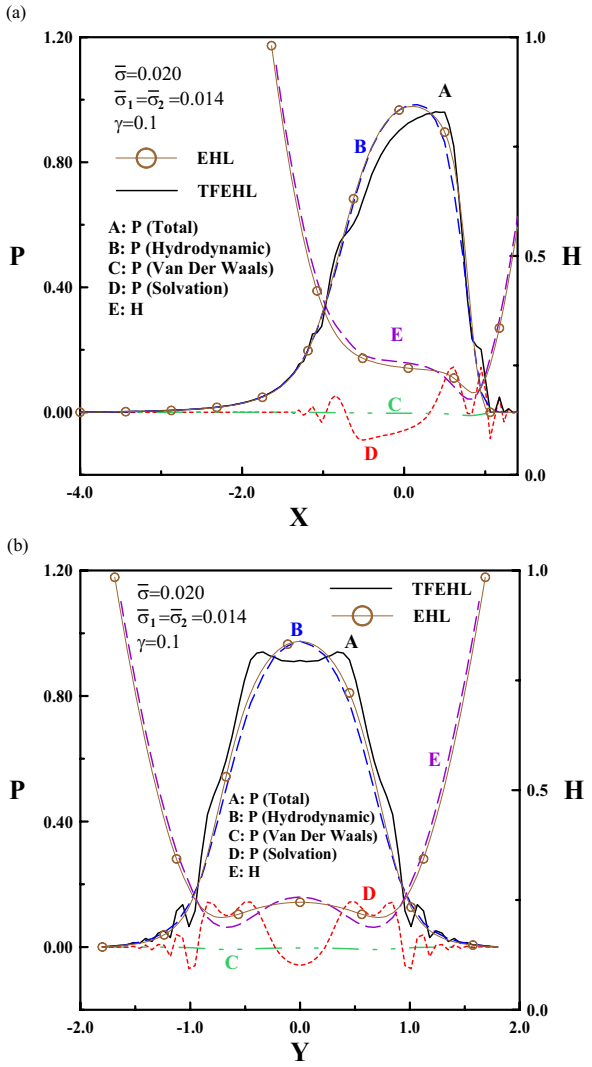

Fig. 4 (colour online). *X*-cross section plot (a) and *Y*-cross section plot (b) of pressure and film shape distributions obtained using two different models.

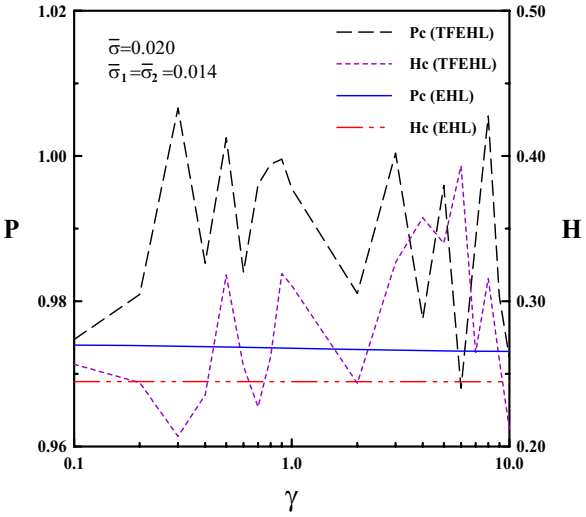

Fig. 5 (colour online). Central pressure and film thickness plotted as functions of Peklenik numbers.

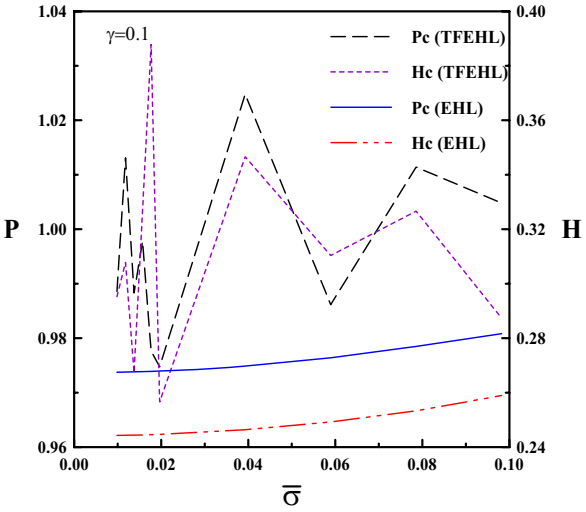

Fig. 6 (colour online). Central pressure and film thickness plotted as functions of composite standard variation.

formation is affected by pressure distributions. Thus, the solvation pressure apparently influences on the film thickness in the Hertzian contact region. The thinner the film thickness is, the greater the difference is.

As shown in Figure 5, the central pressure P_c and central film thickness H_c are plotted as functions of the Peklenik number γ. The central pressure and central film thickness calculated by the classical EHL model decrease as γ increases under constant load condition. But the central pressure and central film thickness oscillate with the Peklenik number by applying the TFEHL model. The central pressure calculated from the TFEHL model is almost larger than that computed from the classical EHL model. The central film thickness calculated from the TFEHL model is between that computed from the classical EHL model.

As shown in Figure 6, the central pressure and central film thickness are plotted as functions of the composite standard deviation $\bar{\sigma}$ of roughness. The central pressure and central film thickness, calculated by

the classical EHL model, increase as $\bar{\sigma}$ increases under constant load condition. But they oscillate with $\bar{\sigma}$ by applying the TFEHL model. The central pressure and film thickness calculated from the TFEHL model is nearly larger than that computed from the classical EHL model.

4. Conclusions

The present analysis investigates the effects of surface roughness and surface force on the TFEHL circular contact problems numerically by solving seven equations simultaneously. In TFEHL problems, the film thickness is usually comparable to the height of surface roughness in the contact zone. Therefore, the effect of surface roughness becomes important. The results show that the differences between the TFEHL model and the EHL model increase with decreasing film thickness. The surface forces have obvious effects in the Hertzian contact region. The oscillation phenomena in pressure and film thickness come mainly from the action of solvation forces. The central pressure and central film thickness oscillate with the Peklenik number and the composite standard deviation of roughness by applying TFEHL model. The central pressure calculated from the TFEHL model is nearly larger than that computed from the classical EHL model.

Acknowledgement

The authors would like to express their appreciation to the National Science Council (NSC 100-2221-E-214-033) in Taiwan for financial support.

[1] G. Guangteng and H. A. Spikes, Tribol. Trans. **39**, 448 (1996).
[2] M. Hartl, I. Krupka, R. Poliscuk, M. Liska, J. Molimard, M. Querry, and P. Vergne, Tribol. Trans. **44**, 270 (2001).
[3] D. Y. C. Chan and R. G. Horn, J. Chem. Phys. **83**, 5311 (1985).
[4] S. Brown and C. Scholz, J. Geophys. Res. **90**, 5531 (1985).
[5] S. Jang and J. Tichy, ASME J. Tribol. **117**, 22 (1995).
[6] H. Matsuoka and T. Kato, ASME J. Tribol. **119**, 217 (1997).
[7] L. S. Ornstein and F. Zernike, Proc. Acad. Sci. Amsterdam **17**, 793 (1914).
[8] J. W. Perram, Mol. Phys. **30**, 1505 (1975).
[9] L. M. Chu, J. Y. Lai, C. H. Chien, and W. L. Li, Tribol. Int. **43**, 523 (2010).
[10] N. Patir and H. S. Cheng, J. Lubric. Tech. Trans. ASME **100**, 12 (1978).
[11] Y. Z. Hu and D. Zhu, ASME J. Tribol. **122**, 1 (2000).
[12] H. Christensen, Proc. Inst. Mech. Eng. **184**, 1013 (1969/70).
[13] H. S. Cheng and A. Dyson, ASLE Trans. **21**, 25 (1978).
[14] J. A. Greenwood and J. H. Tripp, Proc. Inst. Mech. Eng. 185, 625 (1970/71).
[15] D. Zuh and H.S. Cheng, ASME J. Tribol. **110**, 32 (1988).
[16] F. Sadeghi and P. C. Sui, ASME J. Tribol. **111**, 56 (1989).
[17] X. Ai and H. S. Cheng, ASME J. Tribol. **116**, 549 (1994).
[18] G. Xu and F. Sadeghi, ASME J. Tribol. **118**, 473 (1996).
[19] D. Nicholson and N. G. Parsonage, Computer Simulation and the Statistical Mechanics of Adsorption, Academic Press, London 1982.
[20] W. L. Li, C. I. Weng, and J. I. Lue, Tribol. Trans. **39**, 819 (1996).
[21] C. J. A. Roelands, J. C. Vlugter, and H. I. Watermann, ASME J. Basic Eng. **601** (1963).
[22] D. Dowson and G. R. Higginson, Elasto-Hydrodynamic Lubrication, Pergamon Press, Oxford, 88 1966.
[23] A. A. Lubrecht, Ph.D. Thesis University of Twente Enschede (ISBN 90-9001583-3) (1987).
[24] C. H. Venner and A. A. Lubrecht, P. I. Mech. Eng. J.-J. Eng. Tribol. **219**, 303 (2005).
[25] A. Brandt and A. A. Lubrecht, J. Comput. Phys. **90**, 348 (1990).